Directly probing the chirality of Majorana edge states

Yao Lu,[1,2] P. Virtanen,[2] and Tero T. Heikkilä[2]

[1]*Centro de Física de Materiales (CFM-MPC), Centro Mixto CSIC-UPV/EHU, Manuel de Lardizabal 5, E-20018 San Sebastián, Spain*

[2]*Department of Physics and Nanoscience Center, University of Jyväskylä, P.O. Box 35 (YFL), FI-40014 University of Jyväskylä, Jyväskylä, Finland*

(Received 15 November 2021; revised 8 July 2022; accepted 12 July 2022; published 26 July 2022)

We propose to directly probe the chirality of Majorana edge states in 2D topological superconductors using polarization selective photon absorption. When shining circularly polarized light on a 2D topological superconductor in disk geometry, the photons can excite quasiparticles only when the polarization of the light matches the chirality of the Majorana edge states required by the angular momentum conservation. Hence, one can obtain the chirality of the Majorana edge states by measuring the photon absorption rate. We show that the polarization selective photon absorption can also serve as smoking gun evidence of the chiral Majorana edge mode.

DOI: 10.1103/PhysRevB.106.045139

I. INTRODUCTION

Searching for Majorana fermions is an important topic in condensed matter physics because of its potential application in topological quantum computing based on the non-Abelian statistics [1–12]. Recently, the chiral Majorana edge states (CMES) localized at the boundary of a 2D topological SC have attracted much attention [13–18]. However, its identification is challenging due to the neutrality of the zero energy Majorana state.

The probable CMES was first observed in the quantum anomalous Hall (QAH)/SC structure [13]. Tuning the external magnetic field, a half-quantized conductance plateau emerges as a signature of the CMES when the system is driven into a topological superconducting phase [16]. However, it has been shown that there are also other possible origins of the half-quantized conductance plateau [19,20], such as disorder. Another platform realizing the CMES is the ferromagnet/Rashba SC bilayer structure [17,18,21]. In this setup, using scanning tunneling microscopy (STM) and scanning tunneling spectroscopy (STS), finite density of states (DOS) below the superconducting gap was observed only close to the edge of the ferromagnet and this is regarded as a signature of the CMES. Recently, it was proposed that the CMES can generate enhanced local optical response at finite frequencies, [22,23] as the states at nonzero energy can couple to the electromagnetic field. The local optical conductivity scales as the square of the frequency, also distinguishing it from the normal edge states.

Despite the great progress made in investigating the properties of the CMES, the STM and local optical measurement only show finite DOS at low energies but fail to tell whether the low energy mode is a chiral mode propagating only in one direction. The main reason for the difficulty is the neutrality of the zero energy Majorana mode. In QAH materials, the chirality of the topological edge states can be probed by measuring the quantized Hall conductance [24,25]. However, in a topological SC, the zero energy Majorana mode is charge neutral and hence produces no Hall conductance. Instead, the CMES generates a quantized thermal Hall conductance [26,27], which is difficult to measure in experiments. Another proposal to detect the chirality of the CMES by two-tip measurement is also experimentally difficult [28].

In this work, we propose to directly probe the chirality of the CMES using polarization selective photon absorption (PSPA). We consider a topological SC in disk geometry. This setup preserves a rotation symmetry (RS). Thus the Majorana states are labeled by the total angular momentum j rather than the momentum k as in the usual cases [29]. Near zero energy, the CMES always has a linear dispersion $E_j = Cv_M j$, where $C = \pm 1$ is the Majorana chirality and $v_M > 0$ is the Majorana angular speed. Shining circularly polarized light with angular momentum $C_l = \pm 1$ and frequency ω on the sample, a quasiparticle with energy E_j and angular momentum j can absorb a photon and be excited to the state with energy $E_j + \hbar\omega$ and angular momentum $j + C_l$ if $C_l = C$ as shown in Fig. 1. On the other hand, if $C_l \neq C$, this optical excitation is forbidden by angular momentum conservation. Therefore, by measuring the photon absorption, one can directly probe the chirality of the CMES. This effect can hence serve as smoking gun evidence of the CMES. The advantage of this method is that it excludes the possibility of low energy trivial Andreev bound states that would have chirality independent response. Such exclusion cannot be achieved by STM or local optical methods.

II. MODEL

We first consider the simplest model of a 2D topological SC: A 2D spinless chiral p wave SC described by the Hamiltonian [2]

$$H = \sum_{\boldsymbol{k}} \tilde{\Psi}_{\boldsymbol{k}}^{\dagger}\left[\left(\frac{\hbar^2\boldsymbol{k}^2}{2m} - \mu\right)\tau_3 + \frac{\Delta}{k_F}(k_x\tau_1 - Ck_y\tau_2)\right]\tilde{\Psi}_{\boldsymbol{k}}. \quad (1)$$

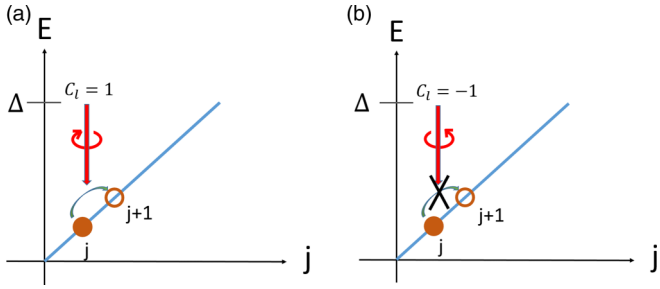

FIG. 1. Schematic energy spectrum of the CMES. (a) A photon can excite a quasiparticle to a higher energy state if $C_l = C$. (b) The optical excitation is forbidden if $C_l \neq C$.

Here $\tilde{\Psi}_{\boldsymbol{k}} = [\psi_{\boldsymbol{k}}, \psi^{\dagger}_{-\boldsymbol{k}}]^{\mathrm{T}}$, where $\psi^{\dagger}_{\boldsymbol{k}}$ is the electron creation operator which creates one electron with momentum $\boldsymbol{k}$. τ is the Pauli matrix acting on the particle-hole space. $C = \pm 1$ is the chirality of the chiral p wave SC. m, μ, and Δ are electron effective mass, chemical potential, and pairing gap, respectively. We consider a sample in disk geometry [30] with the boundary $x^2 + y^2 = R_0^2$, where x and y are spatial coordinates and R_0 is the radius. The energy of the bulk states can be obtained by diagonalizing the Hamiltonian. The bulk spectrum close to $k \approx k_F$ is the usual Bogoliubov spectrum and has the gap Δ. To find the subgap edge states, it is convenient to use the polar coordinates (r, ϕ). This system preserves a generalized RS: $[H, J] = 0$, where $J = -i\partial_\phi - \frac{1}{2}\tau_3$ is the generalized angular momentum operator around the z axis. Thus the total angular momentum j is a good quantum number and the edge states take the form

$$\Psi_{M,j} = e^{ij\phi}\begin{bmatrix} \psi_{+,M,j}(r)e^{i\phi/2} \\ \psi_{-,M,j}(r)e^{-i\phi/2} \end{bmatrix}, \tag{2}$$

where $j = n + 1/2$ with $n \in Z$. Here we assume that the radius R_0 of the sample is much larger than the Majorana localization length and the Fermi wavelength $2\pi/k_F$, where k_F is the Fermi momentum and v_F is the Fermi velocity. By using the hard wall boundary condition $\Psi_j(r = R_0) = [0, 0]^{\mathrm{T}}$, we obtain the energy $E_j = \frac{Cj\Delta}{k_F R_0}$ and the wave function of the low-energy edge states [31]

$$i\psi_{+,M,j} = \psi_{-,M,j} = \frac{1}{\sqrt{2}}\left[e^{\kappa_+(r-R_0)} - e^{\kappa_-(r-R_0)}\right], \tag{3}$$

where $\kappa_\pm = \frac{m}{\hbar^2}\left[\frac{\Delta}{k_F} \pm \sqrt{\frac{\Delta^2}{k_F^2} - \frac{2\hbar^2\mu}{m}}\right]$. One can see that there are low energy states localized at the boundary as long as $\mu > 0$ required by $\mathrm{Re}(\kappa_\pm) > 0$. The effective Majorana angular speed is given by $v_M = \frac{C\Delta}{k_F R_0}$. This shows that the chirality of the CMES is indeed C.

III. OPTICAL RESPONSE

When shining light with a frequency ω much lower than the pairing gap of the sample, the photon can be absorbed by the edge states and excite the quasiparticles to higher-energy states, if selection rules allow it. For circularly polarized light, the vector potential is $\boldsymbol{A} = A(1, iC_l)$, where $C_l = \pm 1$ is the angular momentum (polarization) of the photon. The photon absorption power W can be determined by $W(\omega) = 4\pi A^2\omega^2 R_0^2 \mathrm{Re}[\sigma_{ll}(\omega)]$, where σ_{ll} is the circular optical conductance, given by

$$\mathrm{Re}\,\sigma_{ll}(\omega) = \frac{1}{2\pi^2\omega R_0^2}\sum_{m,n}\langle m|J_l^{\dagger}|n\rangle\langle n|J_l|m\rangle \times \mathrm{Im}\,\frac{f(E_n) - f(E_m)}{E_m - E_n - \hbar\omega + i0^+}, \tag{4}$$

where $|m\rangle$ is the edge eigenstate with angular momentum m, E_m is the eigenenergy, and $f(E)$ is the Fermi distribution function. The generalized current operator J_l is the integral of the current density operator over the volume, given by $J_l = \frac{\hbar e}{m}e^{iC_l\phi}(-i\partial_r + \frac{C_l}{R_0}\partial_\phi)$, where e is the electron charge. With this generalized current operator we can calculate the matrix element in Eq. (4), $\langle m|J_l|n\rangle = \frac{i\hbar e v_F E_n}{\Delta}\delta_{m,n+C_l}$, where $v_F = \hbar k_F/m$ is the Fermi velocity in the normal state. This matrix element has several important features: first, it is proportional to v_F rather than the velocity of the edge states; second, the matrix element is linear in energy E_n in contrast to the case of normal chiral edge states [23]; third, the finiteness of the matrix element depends on the polarization of the light C_l. We get the real part of the optical conductance by substituting the matrix element into Eq. (4) [31],

$$\mathrm{Re}[\sigma_{ll}(\omega)] = \frac{e^2 v_F^2}{2\pi R_0^2\omega\hbar\Delta^2}\sum_j E_j^2[f(E_j) - f(E_{j+1})] \times \delta\left(\omega - \frac{\Delta}{k_F R_0}\right)\delta_{C,C_l}, \tag{5}$$

where f is the Fermi distribution function. In the parameter regime $\hbar\omega \ll k_B T \ll \Delta$, the above equation can be simplified

$$\mathrm{Re}[\sigma_{ll}(\omega)] \approx \frac{\pi^2 e^2 T^2 v_F^2 k_F}{3h\Delta^3 R_0}\delta\left(\hbar\omega - \frac{\Delta}{k_F R_0}\right)\delta_{C,C_l}. \tag{6}$$

One can see that $\mathrm{Re}[\sigma_{ll}(\omega)]$ is nonzero only when $C = C_l$ and $\hbar\omega = \Delta/k_F R_0$ required by the energy conservation and angular momentum conservation. Therefore, by shining circularly polarized light on a 2D topological superconductor one can directly probe the chirality of the CMES via measuring the photon absorption rate. We also note that the effective velocity of the CMES is the Fermi velocity v_F while the density of states of the CMES (N_M) is determined by its group velocity v_M, $N_M \propto 1/v_M$. Therefore, there is a large prefactor v_F^2/v_M^2 in the optical conductance σ_{ll}, resulting in the fact that σ_{ll} can be several orders of magnitude larger than e^2/h.

In systems with a higher Chern number [17], several Majorana edge modes are present. If the velocities of the modes differ, they appear in the photon absorption rate as separate peaks at the frequencies determined by the angular momentum selection rule. If the velocities are too close to each other to be resolved, the low-temperature absorption spectrum provides a lower bound for the number of edge states.

For comparison with Eq. (6), we consider the optical response of normal chiral edge states in a QAH insulator. Note that a QAH insulator can also be described by Eq. (1) with $\tilde{\Psi}$ replaced by $\Psi = (\psi_\uparrow, \psi_\downarrow)^{\mathrm{T}}$, the Pauli matrix τ replaced by the Pauli matrix σ acting on the spin space, and Δ replaced by the spin orbit coupling strength Δ_α [32]. The current operator, however, is different, and the optical conductance is given

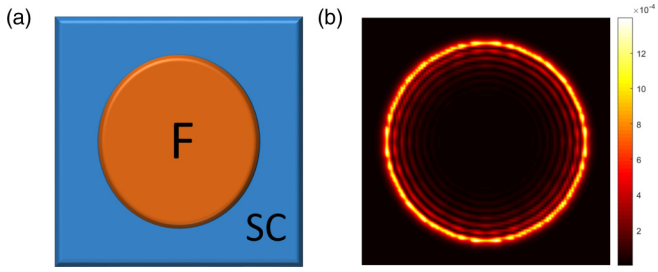

FIG. 2. (a) Sketch of an F/SC structure realizing 2D topological superconductor. (b) Spatial distribution of $|\Psi|^2$, where Ψ is the wave function of the lowest energy state.

by [23]

$$\mathrm{Re}[\sigma_{ll}(\omega)] = \frac{e^2\Delta_\alpha}{hk_FR_0}\delta\left(\hbar\omega - \frac{\Delta_\alpha}{k_FR_0}\right). \tag{7}$$

In the normal state, $\mathrm{Re}[\sigma_{ll}]$ is independent of the temperature. The difference of temperature dependence of the optical conductance is due to the fact that the Majorana excitation is the superposition of electron and hole excitation, so that the Majorana states couple to the external electromagnetic field differently from normal edge states.

A. F/SC lattice model

Recently, there have been several experiments realizing the CMES in a ferromagnet/SC structure as shown in Fig. 2(a). [17,18] This system can be described by the effective tight-binding Hamiltonian

$$H_{TB} = \sum_{\boldsymbol{R},\boldsymbol{d}} t\psi^\dagger_{\boldsymbol{R}+\boldsymbol{d}}\Psi_{\boldsymbol{R}} - \mu\Psi^\dagger_{\boldsymbol{R}}\Psi_{\boldsymbol{R}} - V_z(\boldsymbol{R})\Psi^\dagger_{\boldsymbol{R}}\sigma_z\Psi_{\boldsymbol{R}} + i\alpha\boldsymbol{d}\times\hat{z}\cdot\Psi_{\boldsymbol{R}+\boldsymbol{d}}\boldsymbol{\sigma}\Psi_{\boldsymbol{R}} + \Delta\Psi_{\boldsymbol{R},\uparrow}\Psi_{\boldsymbol{R},\downarrow} + \mathrm{H.c.}, \tag{8}$$

where $\boldsymbol{R}$ denotes the lattice sites, and $\boldsymbol{d}$ denotes the two unit vectors d_x and d_y. t is the hopping strength, μ is the chemical potential, α is the Rashba coefficient, and Δ is the pair potential. $V_z(\boldsymbol{R})$ is a position dependent exchange field $V_z(\boldsymbol{R}) = V_0$ when $|\boldsymbol{R}| < R_0$, and otherwise zero. When $V_0^2 > \mu^2 + \Delta^2$, the ferromagnetic part is topological while the nonmagnetic part is trivial. We get the eigenstates of this tight-binding Hamiltonian by diagonalizing it. The wave function of the eigenstate closest to the zero energy is shown in Fig. 2(b). This subgap state, localized at the boundary of the ferromagnet region, is the chiral Majorana state. In this tight-binding model, the generalized current operator corresponding to circularly polarized light is given by [31]

$$J_l = \frac{ea}{4\pi}\sum_{\boldsymbol{R},q} B_q[it\Psi^\dagger_{\boldsymbol{R}+\boldsymbol{d}_q}\Psi_{\boldsymbol{R}} + \mathrm{H.c.}] - B_q[\alpha\boldsymbol{d}_q\times\hat{z}\cdot\Psi^\dagger_{\boldsymbol{R}+\boldsymbol{d}_q}\boldsymbol{\sigma}\Psi_{\boldsymbol{R}} + \mathrm{H.c.}], \tag{9}$$

where $q = x, y$ and $B_x = 1$, $B_y = i$ and a is the lattice constant. The first term in Eq. (9) comes from the kinetic energy, and the second term is the Rashba contribution. We numerically calculate the optical conductance using Eq. (4), and the results are shown in Fig. 3. When $C_l = 1$, $\mathrm{Re}[\sigma_{ll}]$ is finite and has a peak when the photon frequency matches the energy spacing of the CMES. When $C_l = -1$, $\mathrm{Re}[\sigma_{ll}]$ is close to zero. When increasing the temperature, the conductance peak is enhanced and broadened. This broadness is due to the fact that the energy spacing of the CMES in this lattice model is not constant, as seen in the inset of Fig. 3.

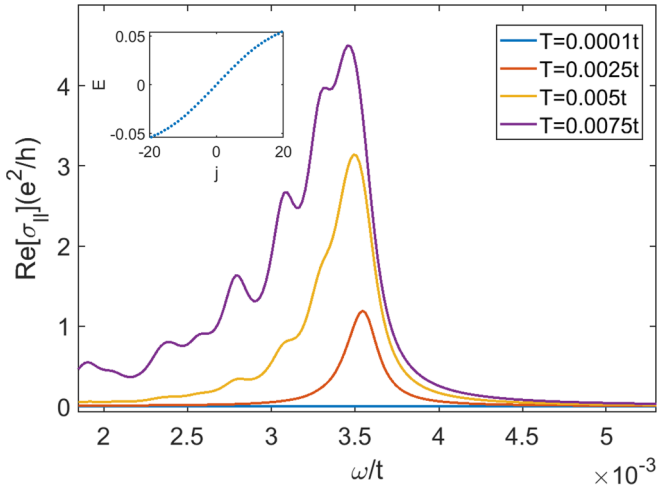

FIG. 3. The real part of the optical conductance as a function of frequency at different temperatures calculated from the lattice model Eq. (8). This figure only shows the optical conductance when $C_l = 1$. For $C_l = -1$, $\mathrm{Re}[\sigma_{ll}]$ overlaps the $C_l = 1$, $T = 0.0025$ curve. The inset shows the nonlinear spectrum of the CMES. Parameters used here are $\Delta = 0.2t$, $\mu = 0t$, $V_0 = 0.5t$, $\alpha = 0.25t$, $R_0 = 40$.

B. Breaking rotation symmetry

So far, we have considered the systems preserving the RS. To investigate how robust the polarization selective photon absorption is against the RS breaking, we first consider a case with nonmagnetic impurities which locally break the RS, but respect the RS on average. We consider the following Hamiltonian:

$$H_{TBD} = H_{TB} - \sum_{\boldsymbol{R}} U(\boldsymbol{R})\Psi^\dagger_{\boldsymbol{R}}\Psi_{\boldsymbol{R}}, \tag{10}$$

where $U(\boldsymbol{R})$ is the disorder potential which is uniformly distributed in $[-U_0, U_0]$. We numerically calculate $\mathrm{Re}[\sigma_{ll}]$ in the presence of $U(\boldsymbol{R})$ and show the results in Fig. 4. It shows that the effect of the disorder is to shift the position of the conductance peak and broaden it. The PSPA survives even when the disorder strength is larger than the pairing gap. This result is expected because the chiral edge states are topologically protected, and hence the PSPA is robust against disorder.

Next we consider an elliptical ferromagnetic island with a boundary described by $bR_x^2 + \frac{1}{b}R_y^2 = R_0^2$. When $b \neq 1$, this geometry does not respect the RS, and the angular momentum is no longer a good quantum number. We numerically calculate $\mathrm{Re}[\sigma_{ll}]$ and show the results in Fig. 5. One can see that, even with a large shape deformation ($b = 2$) which greatly breaks the rotation symmetry (inset of Fig. 5), $\mathrm{Re}[\sigma_{ll}]$ for $C_l = 1$ is much larger than that for $C_l = -1$. This can be understood as follows. Since the Majorana wave function is single valued, we can use an integer-winding number to label the CMES. The circular polarized light with C_l approximately changes the winding number by C_l, and we assume the CMES Ψ_m with

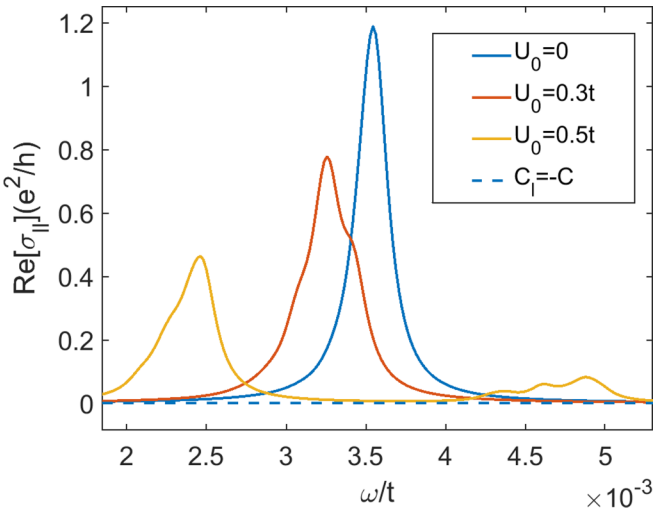

FIG. 4. Real part of the optical conductance as a function of frequency for different disorder strengths. Here we consider one disorder configuration. The solid lines and dashed lines represent $C_l = 1$ and $C_l = -1$, respectively. For $C_l = -1$, Re$[\sigma_{ll}]$ with any disorder strength is much smaller than that of $C_l = 1$ and overlap each other, so we only show one of them in this figure. The parameters used here are as in Fig. 3 with $T = 0.0025t$.

the winding number w roughly satisfies the normalization condition $\langle \Psi_m | \Psi_{m'} \rangle \approx \delta_{m,m'}$. Therefore, similar to the angular momentum conservation, the number conservation" can also approximatively induce PSPA.

C. Experimental detection

Polarized electromagnetic fields can be generated in a cross-shaped rf cavity, [33] as illustrated in Fig. 6. The polarization is controlled by the phase shift ϕ_0 between the sources, $A_x(t) \sim A\,\mathrm{Re}\,e^{i\omega t}$, $A_y(t) \sim A\,\mathrm{Re}\,e^{i\omega t+\phi_0}$, and is circularly polarized if $\phi_0 = \pm\pi/2$. As we have shown, if the

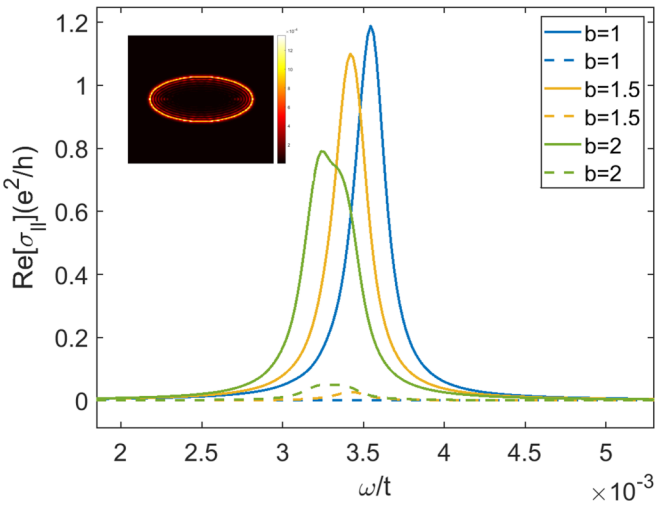

FIG. 5. Real part of the optical conductance as a function of frequency for different shapes. The solid lines and dashed lines represent $C_l = 1$ and $C_l = -1$, respectively. The inset shows the spatial distribution of the lowest energy for $b = 2$. The parameters used here are as in Fig. 3 with $T = 0.0025t$.

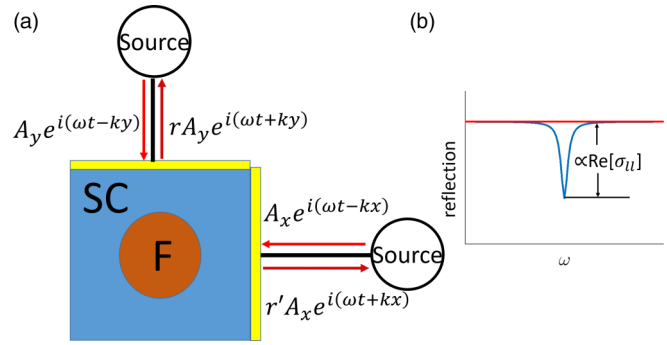

FIG. 6. (a) Setup to probe the chirality of the CMES. Yellow denotes the electrodes. (b) Sketch of the predicted microwave reflection rate as a function of frequency ω. There is a reflection dip when the frequency is equal to the energy spacing of the CMES, and the polarization of the microwave matches that of the Majorana mode (blue line). The reflection rate is independent of the frequency when the polarization of the microwave does not match that of the Majorana mode (red line).

microwave polarization matches the chirality of the CMES, the photon absorption rate is peaked at frequency $\hbar\omega = \delta E$, corresponding to the energy spacing of the CMES. This can be observed as an enhanced absorption peak, whose presence and amplitude depends on ϕ_0 and temperature. The resonant frequency can also be varied *in situ*, since the superconducting gap Δ depends on, e.g., temperature T and applied magnetic field B. The challenge in measuring the absorption peak is that the Majorana conductance is shorted by the large admittance of the host superconductor. On the other hand, as mentioned above, the Majorana edge states can have a large optical conductance far exceeding e^2/h. Using parameters from a recent experiment on 2D Majorana modes [17,31], we estimate that the amplitude of the absorption peak, or a reflection dip in a microwave transmission measurement, can be several percent, making the scheme directly experimentally measurable [34].

IV. CONCLUSIONS

We have shown that, when shining circularly polarized light onto a 2D topological superconductor with subgap CMES, the photon absorption rate is finite only when the polarization of the light matches the chirality of the CMES. We propose that this effect can be used to directly probe the chirality of the CMES. We show that this selective photon absorption effect is robust against rotation symmetry breaking, such as disorder or shape deformation.

ACKNOWLEDGMENTS

We thank Shawulienu Kezilebieke, Mika Sillanpä and Juha Muhonen for discussions. This work was supported by the Academy of Finland (Project No. 317118). It has also received funding from the European Union's Horizon research and innovation programme under Grant Agreement No. 800923. We acknowledge grant PID2020-114252GB-I00 (SPIRIT) funded by MCIN/AEI/10.13039/501100011033 and by "ERDF A way of making Europe". This work is funded by the Education Department of the Basque Government via the IKUR strategy program. 20-114252GB-I00 (SPIRIT).

[1] A. Y. Kitaev, Phys. Usp. **44**, 131 (2001).
[2] X.-L. Qi and S.-C. Zhang, Rev. Mod. Phys. **83**, 1057 (2011).
[3] L. Fu and C. L. Kane, Phys. Rev. Lett. **100**, 096407 (2008).
[4] J. D. Sau, R. M. Lutchyn, S. Tewari, and S. DasSarma, Phys. Rev. Lett. **104**, 040502 (2010).
[5] K. T. Law, P. A. Lee, and T. K. Ng, Phys. Rev. Lett. **103**, 237001 (2009).
[6] V. Mourik, K. Zuo, S. M. Frolov, S. Plissard, E. P. Bakkers, and L. P. Kouwenhoven, Science **336**, 1003 (2012).
[7] S. Nadj-Perge, I. K. Drozdov, J. Li, H. Chen, S. Jeon, J. Seo, A. H. MacDonald, B. A. Bernevig, and A. Yazdani, Science **346**, 602 (2014).
[8] S. D. Sarma, M. Freedman, and C. Nayak, npj Quantum Inf. **1**, 15001 (2015).
[9] Y. Lu, W.-Y. He, D.-H. Xu, N. Lin, and K. T. Law, Phys. Rev. B **94**, 024507 (2016).
[10] S. Manna, P. Wei, Y. Xie, K. T. Law, P. A. Lee, and J. S. Moodera, Proc. Natl. Acad. Sci. USA **117**, 8775 (2020).
[11] M. Ezawa, Phys. Rev. B **102**, 075424 (2020).
[12] B. Lian, X.-Q. Sun, A. Vaezi, X.-L. Qi, and S.-C. Zhang, Proc. Natl. Acad. Sci. USA **115**, 10938 (2018).
[13] Q. L. He, L. Pan, A. L. Stern, E. C. Burks, X. Che, G. Yin, J. Wang, B. Lian, Q. Zhou, E. S. Choi *et al.*, Science **357**, 294 (2017).
[14] Y. Lu, P. Virtanen, and T. T. Heikkilä, Phys. Rev. B **102**, 224510 (2020).
[15] X.-L. Qi, T. L. Hughes, and S.-C. Zhang, Phys. Rev. B **82**, 184516 (2010).
[16] J. Wang, Q. Zhou, B. Lian, and S.-C. Zhang, Phys. Rev. B **92**, 064520 (2015).
[17] S. Kezilebieke, M. N. Huda, V. Vaňo, M. Aapro, S. C. Ganguli, O. J. Silveira, S. Godzik, A. S. Foster, T. Ojanen, and P. Liljeroth, Nature (London) **588**, 424 (2020).
[18] A. Palacio-Morales, E. Mascot, S. Cocklin, H. Kim, S. Rachel, D. K. Morr, and R. Wiesendanger, Sci. Adv. **5**, eaav6600 (2019).
[19] W. Ji and X.-G. Wen, Phys. Rev. Lett. **120**, 107002 (2018).
[20] Y. Huang, F. Setiawan, and J. D. Sau, Phys. Rev. B **97**, 100501(R) (2018).
[21] A. Yamakage, Y. Tanaka, and N. Nagaosa, Phys. Rev. Lett. **108**, 087003 (2012).
[22] J. J. He, Y. Tanaka, and N. Nagaosa, Phys. Rev. Lett. **126**, 237002 (2021).
[23] J. J. He and N. Nagaosa, Phys. Rev. B **103**, L241109 (2021).
[24] C.-Z. Chang, J. Zhang, X. Feng, J. Shen, Z. Zhang, M. Guo, K. Li, Y. Ou, P. Wei, L.-L. Wang *et al.*, Science **340**, 167 (2013).
[25] C.-X. Liu, S.-C. Zhang, and X.-L. Qi, Annu. Rev. Condens. Matter Phys. **7**, 301 (2016).
[26] H. Sumiyoshi and S. Fujimoto, J. Phys. Soc. Jpn. **82**, 023602 (2013).
[27] Y. Shimizu, A. Yamakage, and K. Nomura, Phys. Rev. B **91**, 195139 (2015).
[28] A. Ptok, D. J. Alspaugh, S. Głodzik, A. Kobiałka, A. M. Oleś, P. Simon, and P. Piekarz, Phys. Rev. B **102**, 245405 (2020).
[29] V. T. Phong, N. R. Walet, and F. Guinea, Phys. Rev. B **96**, 060505(R) (2017).
[30] M. Stone and R. Roy, Phys. Rev. B **69**, 184511 (2004).
[31] See Supplemental Material at http://link.aps.org/supplemental/10.1103/PhysRevB.106.045139 for derivations for eigen-states of a p wave superconductor in disk geometry, the calculation of optical conductance of the CMES in a p wave superconductor, derivations for current operator in the tight binding model, and estimation of microwave reflection coefficient. This includes a reference to X. Xi, Z. Wang, W. Zhao, J.-H. Park, K.T. Law, H. Berger, L. Forró, J. Shan, and K. F. Mak, Nat. Phys. 12, 139 (2016).
[32] X.-L. Qi, Y.-S. Wu, and S.-C. Zhang, Phys. Rev. B **74**, 085308 (2006).
[33] T. P. Mayer Alegre, C. Santori, G. Medeiros-Ribeiro, and R. G. Beausoleil, Phys. Rev. B **76**, 165205 (2007).
[34] R. Haller, G. Fülöp, D. Indolese, J. Ridderbos, R. Kraft, L.Y. Cheung, J.H. Ungerer, K. Watanabe, T. Taniguchi, D. Beckmann, R. Danneau, P. Virtanen, and C. Schonenberger, Phys. Rev. Research **4**, 013198 (2022).